Applied Catalysis B: Environmental 336 (2023) 122915

Contents lists available at ScienceDirect

Applied Catalysis B: Environmental

journal homepage: www.elsevier.com/locate/apcatb

# Activation of molecular oxygen over binuclear iron centers in Al-rich *BEA zeolite

Agnieszka Kornas [a], Edyta Tabor [a], Dominik K. Wierzbicki [b,c], Joanna E. Olszowka [a], Radim Pilar [a], Jiri Dedecek [a], Michal Sliwa [d], Hana Jirglova [a], Stepan Sklenak [a], Dorota Rutkowska-Zbik [d], Kinga Mlekodaj [a,*]

[a] J. Heyrovský Institute of Physical Chemistry of the Czech Academy of Sciences, v. v. i., Dolejškova 2155/3, 182 23 Prague 8, Czech Republic
[b] Paul Scherrer Institute, Forschungsstrasse 111, 5232 Villigen PSI, Switzerland
[c] AGH University of Science and Technology, Faculty of Energy and Fuels, Al. A. Mickiewicza 30, 30–059 Kraków, Poland
[d] Jerzy Haber Institute of Catalysis and Surface Chemistry, Polish Academy of Sciences, Niezapominajek 8, 30–239 Kraków, Poland

ARTICLE INFO

*Keywords:*
Molecular oxygen splitting
Distant binuclear iron centers
Methane oxidation
Al-rich *BEA
Template-free synthesis

ABSTRACT

Here, we present the unique redox properties of distant binuclear iron centers in Al-rich *BEA zeolite in $O_2$ splitting and $CH_4$ oxidation. Al-rich *BEA was obtained via a template-free synthesis procedure guaranteeing low-defected structure and a high fraction of Al-pairs enabling stabilization of binuclear iron centers. By employment of a multispectroscopic in-situ approach (Mössbauer and X-ray absorption) the formation of active oxygen over binuclear iron centers in Al-rich *BEA was confirmed and subsequent $CH_4$ oxidation was studied. Spontaneous release of the reaction products to the gas stream, representing a significant advantage of the studied system, was proved by the results of in-situ FTIR and mass spectrometry. This is the first experimental proof of the formation of fully-functioned binuclear iron centers (able to split $O_2$, stabilize active oxygen forms, and subsequently oxidize $CH_4$) in zeolite of *BEA topology.

## 1. Introduction

The employment of molecular oxygen as an eco-friendly and easily accessible oxidant for important processes is a challenge for environmental catalysis on its path to sustainability. [1] However, the most demanding step when using molecular oxygen is its activation, which so far was carried out most effectively over metalloenzymes in biological systems [2–4]. Nature teaches us that in enzyme the cooperation of two cations of transition metal ions (TMI) as an active center is required to split molecular oxygen into its active form, which can be further utilized in the oxidation of such inert organic compounds as methane [5–7]. Methane features in high activation energy of four equal C-H bonds (101 kcal/mol), high symmetry, and low polarizability, altogether making it chemically stable [8]. So far, the only commercial way for methane utilization was steam reforming resulting in obtaining the syngas, which can be further transformed into methanol. The latter is considered as desired energy vector; however, its production via the syngas process is highly demanding and requires significant economic and energetic outlays. Enzymes can perform oxidation of methane at the cellular level, however currently we are facing the excess of methane on a global scale, and the development of an efficient catalytic system is needed to transform methane into oxygen-containing compounds representing the platform for chemical production and possible energy vector [9]. In metallozeolites, being inorganic analogs of enzymes [1,3,7,10–13], TMI serving as redox active centers are embedded in a 3D crystalline, porous aluminosilicate matrix [10,14–16]. Zeolites, due to the partial substitution of Si atoms with Al ones resulting in formation of negative charge of the matrix offer the possibility to stabilize TMI in cationic positions with an open, and easily accessible for reactants coordination sphere [14–17]. Recently discovered distant binuclear divalent iron centers located in close vicinity across the zeolite channel of ferrierite (FER) topology are capable of proceeding four electrons redox cycle (Fe(II) ↔ Fe(IV)) with oxidants such as $N_2O$ or $O_2$ [18–20]. The interaction of binuclear Fe(II) centers in FER with $N_2O$ or $O_2$ leads to the formation and stabilization of the active oxygen form, so-called α- oxygen (α-O) [3,10,17,18,20]. The outstanding feature of these α-O species is their ability to attack the strong C-H bond of inert $CH_4$ molecules with the production of oxygenates, including methanol, or stabilization of

* Corresponding author.
*E-mail address:* kingapatrycja.mlekodaj@jh-inst.cas.cz (K. Mlekodaj).

https://doi.org/10.1016/j.apcatb.2023.122915
Received 31 October 2022; Received in revised form 4 April 2023; Accepted 23 May 2023
Available online 24 May 2023

methoxy species bound to the zeolite framework [1,3,9,14–16,18–20].

The mechanism of α-O formation from molecular oxygen over binuclear iron centers in FER significantly differs from the one suggested for Cu-zeolite catalysts also studied in methane to methanol oxidation [21]. In the case of binuclear iron centers in FER, the $O_2$ splitting is possible due to the cooperation of two axially arranged Fe(II) ions through the zeolitic channel at the proper distance of 7.5 Å [18,19]. Conversely, the Cu-based system activates molecular oxygen via the formation of the oxygen bridge between two copper ions distanced by 3.5 Å [22,23]. The oxidation of methane using Cu-oxo bridging species is, according to DFT modeling, inherently connected with strong ligation of the oxo-products to the active site and the need for their extraction by water vapor at elevated temperature [23]. Moreover, the application of the water extraction results in possible poisoning of the Cu-precursor of the active site by water molecules. On the contrary, α-O species (originating from both $N_2O$ and $O_2$) stabilized on the cooperating binuclear TMI centers in FER perform oxidation of methane, and the oxidation products are released directly to the gas phase, without using any effluent [17,19,20]. Eventually, similar properties were recently observed by other scientific groups for Fe-FER and also Fe-CHA zeolites in methane oxidation by α-O from $N_2O$ [11].

Based on recent studies, binuclear TMI centers are the most effective active sites for carrying both, the activation of molecular oxygen and the subsequent methane oxidation. However, their functionality was so far confirmed exclusively in the FER topology. Nevertheless, a DFT study predicted that iron cations can form binuclear centers in other than FER zeolitic topologies when cationic positions for divalent cations are properly arranged by facing each other axially in close vicinity (7–9 Å) [18]. Among the suggested zeolitic topologies wide-pore *BEA was mentioned (Fig. 1a) with the energy barrier of molecular oxygen splitting of 31 kcal/mol [18] (Fig. 1b, c); yet the formation of distant binuclear TMI centers requires not only proper arrangement of zeolite rings forming cationic positions but also a proper organization of Al atoms in the zeolite framework. In Si-rich zeolites, three types of Al atoms arrangements can be distinguished [24]: (i) Al pairs, which correspond to two Al atoms located in one zeolite ring, accommodating bare divalent cations (in the case of *BEA and FER zeolites, it means AlSiSiAl sequences located in one 6-membered ring of so-called α- and β-cationic positions); (ii) single Al atoms, which can host only monovalent species; (iii) close Al atoms, reported for *BEA zeolite, which can stabilize only hydrated complexes of divalent TMI [25] (in *BEA, this type of Al distribution corresponds to two Al atoms in the AlSiSiSiAl sequence located in two different rings). Moreover, for Al-rich *BEA zeolites also AlSiAl sequences located across the zeolite wall were reported [24,26]. Al atoms in such sequences are facing different channels, and thus can behave either as Al pairs or close Al atoms. Very recently described synthesis protocol of *BEA leads to a promising material with a high Al population in the framework, offering a sufficient potential fraction of Al pairs needed for the formation of binuclear centers [27–29]. Moreover, the developed protocol for obtaining these Al-rich *BEA materials meets the requirements of sustainable catalyst production due to the template-free approach, which in addition guarantees a low-defected structure [30,31]. It is due to the lack of the necessity of the calcination step, which in the case of *BEA material very often results in the dealumination of parent material and the formation of undesired extra-framework Al species [30,31]. The formation of distant binuclear iron centers in *BEA topology (3D large pore with 12-membered ring channel system) is of high importance for oxidation catalysis as it opens the possibility to apply molecular oxygen as an oxidant for the transformation of not only methane but also bulkier molecules.

In this work, we experimentally confirm for the first time the formation of distant binuclear iron centers in the Al-rich zeolite matrix of *BEA topology. The fully-functioned binuclear iron centers in *BEA are able to split molecular oxygen to a pair of α-oxygen species, and subsequently, oxidize methane to oxygen-containing products detected directly in the gas stream without the extraction step. For this purpose, we employed newly synthesized Al-rich *BEA material with a low-defected structure guaranteed by the template-free, eco-friendly synthesis protocol and a high population of Al pairs in its framework as support to introduce distant binuclear iron centers. Moreover, the pioneering studies of the speciation of iron and its redox properties in the Al-rich *BEA system were carried out under in-situ conditions using Mössbauer and X-ray absorption spectroscopy. The employment of these methods allowed the establishment of the spectroscopic benchmarks of the iron species present in Al-rich *BEA and compare them with the structures of active centers predicted by DFT studies. Moreover, the oxidation properties of α-O stabilized over binuclear iron centers in Al-rich *BEA towards methane oxidation were determined for the first time, and potential reaction products were monitored by FTIR spectroscopy and mass spectrometry. Oxidation of highly resistant $CH_4$ molecule was used as a test reaction of activity of the previously formed α-oxygen.

## 2. Experimental section

### 2.1. Synthesis

Al-rich *BEA zeolite was synthesized hydrothermally from aluminosilicate mixtures of molar compositions 0.13 $Al_2O_3$: 1 $SiO_2$: 0.4 NaOH: 8 $H_2O$ without an organic template but with the addition of seeds of BEA zeolite Si/Al 11.5 (Lot. # TZB-212, Tricat). The synthesis mixture was placed in Teflon-lined stainless-steel autoclaves at 120 °C for 5 days. The

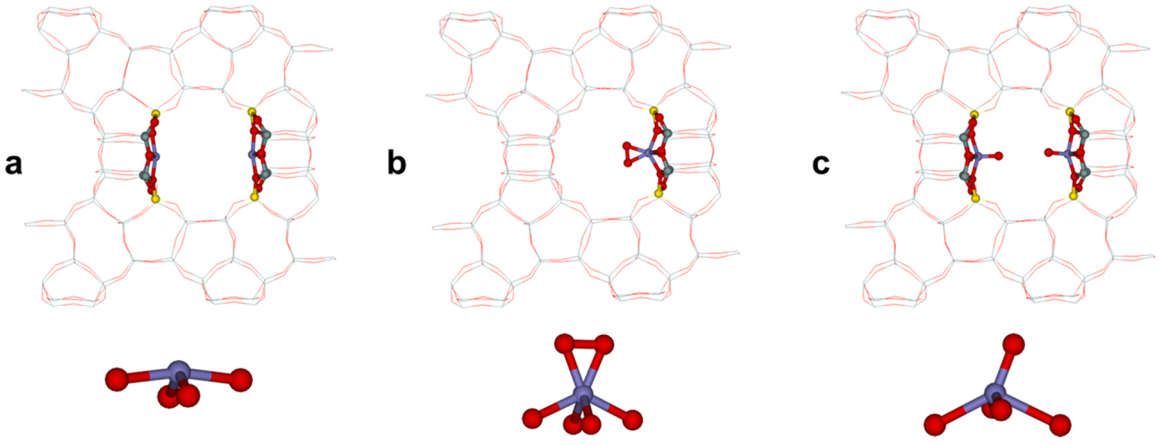


**Fig. 1.** Arrangement of binuclear Fe(II) site in the beta zeolite (a), isolated Fe(II) site in the beta zeolite with the bidentate adsorbed oxygen molecule (b), and of its oxidized form (c), together with the corresponding coordination/geometry of iron ions.

obtained sample was thoroughly washed and dried [31].

### 2.2. Introduction of transition metal ions

In order to study Al distribution in Al-rich *BEA zeolite, part of the as-made sample was ion-exchanged with 0.05 M solution of $Co(NO_3)_2$ (3 ×24 h,100 $cm^3$ of the solution per 1 g of the sample) to achieve fully loaded Co-containing sample [24].

Fe-containing samples (Fe/Al 0.1) were obtained via the impregnation method described elsewhere [32–34]. For this purpose, 2 g of the remaining material (as made) was transferred into its $NH_4$-form by repeated ion exchange with 1 M solution of $NH_4NO_3$, then granulated (fraction of 0.3–0.6 mm), dried, and finally mixed with a solution of $FeCl_3$ (0.25 g) dissolved in acetylacetone (7 g). Next, the sample was subdued to gradual heating (1 h at 100 °C, then 3 h at 350 °C) under a dynamic vacuum. After cooling down, the sample was washed with distilled water and calcined in air at 450 °C.

For the Mössbauer study, an Al-rich $^{57}$Fe-*BEA with Fe/Al 0.06 was prepared by the same procedure by using $^{57}$Fe isotope ($^{57}$Fe > 98 wt% in $Fe_2O_3$, supplied by ISOFLEX, USA). $^{57}Fe_2O_3$ was transferred to $^{57}FeCl_3$, which was used for the preparation of the impregnation solution. This preparation method and employment of $^{57}$Fe as a source of iron species allows to analyze all iron sites stabilized in $^{57}$Fe-*BEA.

### 2.3. Structural analysis

**X-ray diffraction** was performed on a Siemens D5005 Powder Diffractometer to confirm the structure typical for Al-rich *BEA zeolite in the obtained material.

**Chemical analysis** of as-made and metal-containing samples was performed based on X-ray fluorescence spectra obtained on a BRUKER AXS S8 Tiger spectrometer. Measured data sets were evaluated using the Spectra plus V3 software for semiquantitative determination of elements from fluorine to uranium with a 5 − 10% error. Data from the chemical analysis were gathered in Table 1.

**Scanning Electron Microscope** images of the as-made *BEA zeolite were obtained with a Hitachi S-4800 instrument and approximate crystal size was determined by using internal software.

**$^{27}$Al MAS NMR, $^{29}$Si MAS NMR, and $^{29}$Si CP MAS NMR** spectra of the studied as made Al-rich *BEA zeolite (already in Na-form) were recorded on a Bruker Avance III 500 WB/US spectrometer at 11.7 T. For this purpose, 3.2 mm and 4 mm $ZrO_2$ rotors with the rotational speed of 20 kHz and 7 kHz were used for $^{27}$Al and $^{29}$Si experiments, respectively. To allow quantitative evolution of the spectra high-power decoupling pulse sequences were used with excitation pulse π/12 (0.7 μs) for $^{27}$Al, and π/2 (4.2 μs) for $^{29}$Si. In the case of the $^{29}$Si cross-polarization (CP) spectra (see Supplementary material, Fig. S1), pulse sequences with a 50% ramp CP pulse, 2000 μs contact time, high-power decoupling, and 5 s relaxation delays were employed. The chemical shifts were referenced to an aqueous solution of Al nitrate for the $^{27}$Al MAS NMR experiments, and $Q_8M_8$ for the $^{29}$Si MAS NMR experiments. DM fit software was applied for the simulation of the $^{29}$Si MAS NMR spectra.

Based on the single pulse $^{29}$Si MAS NMR spectra, the framework aluminum content ($Si/Al_{FR}$) was calculated by using the following equation (1):

$$\mathrm{Si}\Big/\mathrm{AlFR} = 1\Big/\sum_n\left(\frac{1}{4}In\right) \quad (1)$$

in which $I_n$ stands for the intensity of the resonance of the Si(4-nSi, nAl) atoms and $I$ is the total $^{29}$Si intensity [35,36].

### 2.4. Analysis of Al distribution

A fully loaded Co-containing *BEA sample prepared under conditions that guarantee the exclusive presence of Co(II) hexaaqua complexes in the ion-exchanged sample was used for the determination of Al distribution in the studied *BEA zeolite according to the method described elsewhere [24,37,38]. In general, Al pairs are able to stabilize Co(II) cation in the hydrated (Co(II) hexaaqua complex) and dehydrated zeolite (bare Co(II)), and their concentration corresponds to the concentration of the latter calculated from FTIR study and is given by the following equation (2):

$$\left[Al_{pair}\right] = 2 \times \left[Co(II)_{bare}\right] \quad (2)$$

Close Al atoms accommodate only Co(II) hexaaqua complex in hydrated zeolites, thus their concentration can be calculated based on the maximum ion-exchange capacity of Co(II) from chemical analysis decreased by the fraction of bare Co(II) stabilized by Al pairs, which is given by the following equation (3):

$$[Al_{close}] = 2 \times [Co(II)] - \left[Al_{pair}\right] \quad (3)$$

Single Al atoms do not participate in the stabilization of divalent cations or their complexes, and can be calculated based on the following equation (4):

$$\left[Al_{single}\right] = [Al] - 2 \times [Co(II)\,] = [Al] - \left[Al_{pair}\right] - [Al_{close}] \quad (4)$$

In order to determine the concentration of bare Co(II) in the sample, static infrared spectra of the Co-containing sample were recorded using an FTIR spectrometer (Nicolet 6700) equipped with a liquid-nitrogen-cooled MCTB detector. The quartz cell with KBr windows was connected to a vacuum, which allowed the transport of the sample between the heating and measurement modes. A thin, self-supporting wafer was placed in the holder and evacuated before the measurement under a dynamic vacuum ($10^{-3}$ Pa) at 450 °C for 3 h. FTIR spectra were recorded at RT in the range between 4 000 and 400 $cm^{-1}$ (128 scans, resolution of 2 $cm^{-1}$). Spectra were normalized regarding the wafer density [39].

The concentration of bare Co(II) in the studied *BEA sample was established based on a method reported elsewhere [30,40]. Spectra in the range of the T-O-T vibrations (970–870 $cm^{-1}$) were deconvoluted using Origin 8.1 software (OriginLab, Northampton, MA) into three Gaussian bands [41]. Further, the modified Beer-Lambert-Bouger law was used for the calculation according to the following equation (5):

$$A = \varepsilon \cdot C \quad (5)$$

where A (cm $g^{-1}$) is the integral intensity of the band normalized to self-

**Table 1**
Chemical composition of obtained Al-rich *BEA sample, fully exchanged by Co(II) based on chemical analysis and FTIR studies, together with the results of Al distribution, and the concentration of introduced iron.

| Sample | Si/Al[a] | Fe/Al[a] | Fe[a] (mmol/g) | Co/Al[a] | $Co_{bare}$/Al[b] | Al[a] (mmol/g) | Co (II)[a] | Co (II)[b]bare | $Al_{pair}$ | $Al_{close}$ | $Al_{single}$ | $Al_{pair}$ (%) | $Al_{close}$ | $Al_{single}$ |
|---|---|---|---|---|---|---|---|---|---|---|---|---|---|---|
| Al-rich Co-*BEA | 5.2 | 0.05 | 0.13 | 0.48 | 0.15 | 2.48 | 1.20 | 0.37 | 0.74 | 1.64 | 0.1 | 30 | 66 | 4 |

[a] Based on XRF
[b] Based on FTIR studies

supporting wafer density, ε is the extinction coefficient (cm μmol$^{-1}$), and C is the concentration of (mmol g$^{-1}$) of bare Co(II).

### 2.5. Mössbauer spectroscopy measurements

The absorption $^{57}$Fe Mössbauer spectra were acquired with a 57 °C source in the Rh matrix (the maximum velocity of the source was 12 mm/s). The velocity scale was calibrated using α-Fe foil. A self-supporting pellet (100 mg) of $^{57}$Fe-*BEA (Al-rich) was placed into the quartz set-up enabling sample transport between the heating and measurement regions and exposition of the samples to various atmospheres of the reactants. Mössbauer spectra were measured at RT under vacuum ($10^{-3}$ Pa) after the following treatments: evacuation under dynamic vacuum for 3 h at 450 °C and evacuation under dynamic vacuum for 3 h at 450 °C, then interaction with $O_2$ (101325 Pa) at 220 °C for 60 min and subsequent 5 min $O_2$ desorption at 220 °C. The spectra were deconvoluted into Lorentzian-shaped components using MossWinn software. The corresponding Mössbauer parameters, i.e. isomer shift (IS) and quadrupole splitting (QS) were then ascribed to individual iron species in Fe-*BEA (Al-rich) [42].

### 2.6. X-ray absorption measurements

Fe K-edge (7.112 keV) X-ray absorption spectra of Al-rich Fe-*BEA were acquired in the transmission mode at the SuperXAS beamline of the Swiss Light Source, Paul Scherrer Institute, Switzerland with the use of Si(111) monochromator and spot size of 2000 × 400 μm$^2$. The Si(111) monochromator crystal, results in an energy resolution of ca. 1.43 × $10^{-4}$ deltaE/E, corresponding to an incoming beam energy bandwidth of ca. 1 eV at 7 keV. A spectrum of Fe reference foil was acquired simultaneously for the energy calibration. Fe-*BEA sample was measured in quartz capillary (10 μm wall thickness and 1.5 mm of external diameter) connected with a gas-flow controlling system and mass spectrometer. XAS spectra were recorded during Fe-*BEA (i) heating in He flow (5 ml/min) up to 450 °C and equilibrating at this temperature for 2 h, (ii) cooling down in He flow (5 ml/min) up to 220 °C, (iii) interaction with $O_2$ (5 ml/min) at 220 °C for 60 min, (iv) interaction of the oxidized sample with $CH_4$ (5 ml/min) at 220 °C for 30 min. Quick-XAS spectra were averaged, background corrected, and normalized using the ProQEXAFS software [43]. EXAFS fitting was performed using the Artemis interface of the Demeter software [44].

### 2.7. Analysis of the reaction products

#### 2.7.1. FTIR spectroscopy

FTIR spectra of the products of methane oxidation by active oxygen stabilized on iron centers in Al-rich *BEA sample were recorded on GC-IR Interface with liquid nitrogen cooled MCT-A detector using Nicolet NEXUS 670 FT-IR spectrometer with a resolution 2 cm$^{-1}$ and 32 scans. The sample in a form of a self-supporting palette (ca. 10 mg/cm$^3$) was placed in the through-flow cell with NaCl windows. Fe-*BEA zeolite before the experiment was pretreated in He flow (100 ml/min, purity 5.0) for 3 h at 450 °C, then oxidized for 60 min in $O_2$ flow (30 ml/min, purity 5.0), and flushed by He (100 ml/min, purity 5.0) for 5 min before the $CH_4$ (5 ml/min, purity 5.5) was introduced at 220 °C for 20 min. A blank experiment with no $O_2$ usage was performed as follows. Fe-*BEA zeolite was pretreated in a flow of pure He (100 ml/min, purity 5.0) at 450 °C for 3 h and then cooled down in He flow to 220 °C then He flow was switched to $CH_4$ flow (5 ml/min, purity 5.5) for 20 min.

#### 2.7.2. Mass spectrometry

The quantitative analysis of the products of methane oxidation by active oxygen formed over Fe-*BEA was performed by AutoChem system (Micromeritics) equipped with a quadrupole mass spectrometer (OmniStarTM Pfeiffer Vacuum). The 0.020 g (fraction of 0.03–0.06 cm) of the Fe-*BEA was placed in the quartz reactor and activated in a He flow (40 ml/min, purity 5.0) for 3 h at 450 °C. Then, the sample was cooled down in He flow to 220 °C, treated at this temperature with $O_2$ (20 ml/min, purity 5.0) for 60 min, and purged with He (5 ml/min, purity 5.0) for 15 min in order to remove the excess of $O_2$. Finally, the oxidized sample interacted at 220 °C with $CH_4$ (5 ml/min, purity 5.5) for 30 min. The signal with $m/z = 31$ and 44 related to methanol and $CO_2$ was analyzed as the only oxidation products in three consecutive redox cycles performed isothermally at 220 °C. After each interaction with $CH_4$, the sample was purged with He (20 ml/min, purity 5.0) for 15 min. The quantitative analysis of produced methanol, and $CO_2$ was based on a calibration using signals $m/z = 31$ and 44 respectively, and injections of a set of different amounts of these chemical compounds and corrected for the pressure changes and mass spectrometer responses during the blank experiment. A blank experiment with quartz wool was performed and did not reveal the significant presence of any $m/z$ signals that can be assigned to products of methane oxidation (Supplementary material, Fig. S7). Also, a blank experiment with the *BEA precursor without introduced iron was performed, and the registered mass spectrum (not showing the presence of oxygenates) was added to the Supplementary material (Fig. S11).

## 3. Results and discussion

### 3.1. Structural characterization of parent Al-rich *BEA zeolite

The XRD patterns, depicted in Fig. 2, show that the obtained parent zeolite exhibit reflexes typical for a well-developed *BEA zeolite with no phase impurities, and in agreement with data previously published for Al-rich *BEA materials [25,31,42]. As visible in SEM micrographs shape of crystals is homogeneous and their average size reaches 0.4 μm (see Fig. 3). The crystal size is significantly bigger than typically reported for commercial or Si-rich *BEA zeolites and corresponds to those already reported for Al-rich *BEA zeolites [25,30,31,42].

### 3.2. Aluminum organization in parent Al-rich *BEA zeolite

$^{27}$Al MAS NMR spectrum, Fig. 4, exhibits only one symmetric signal with an observed shift around 58 ppm confirming the exclusive presence of tetrahedrally coordinated Al atoms in an oxygen environment, typical for framework Al atoms with no resonances around 0 or 10 – 40 ppm reflecting the presence of extra-framework Al species. $^{29}$Si MAS NMR spectrum is more complex comparing those reported for Si-rich *BEA zeolites due to the presence of resonances associated with the abundant Si atoms with more than one neighboring Al atom, which is characteristic for Al-rich *BEA zeolite [24,25,45], see Fig. 5. Resonances at − 114.2 and − 109.0 ppm were assigned to Si atoms with the exclusive

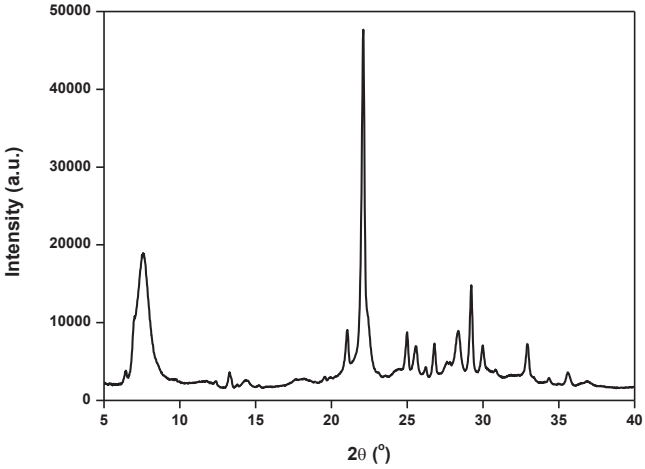


**Fig. 2.** XRD pattern of the as-made Al-rich *BEA zeolite.

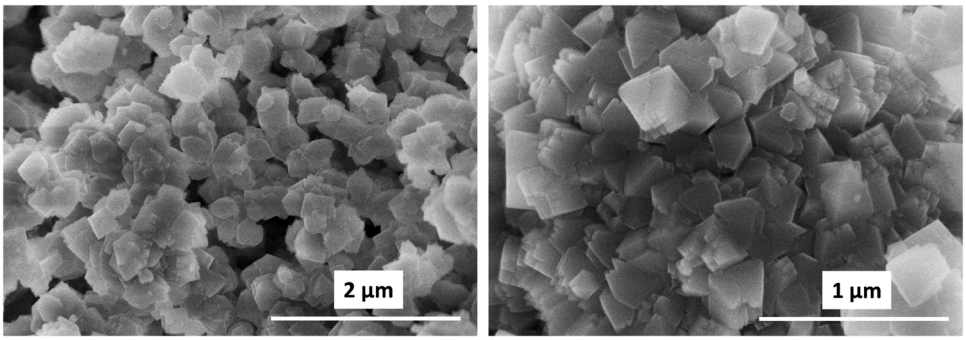


**Fig. 3.** SEM images of as-made Al-rich *BEA zeolite.

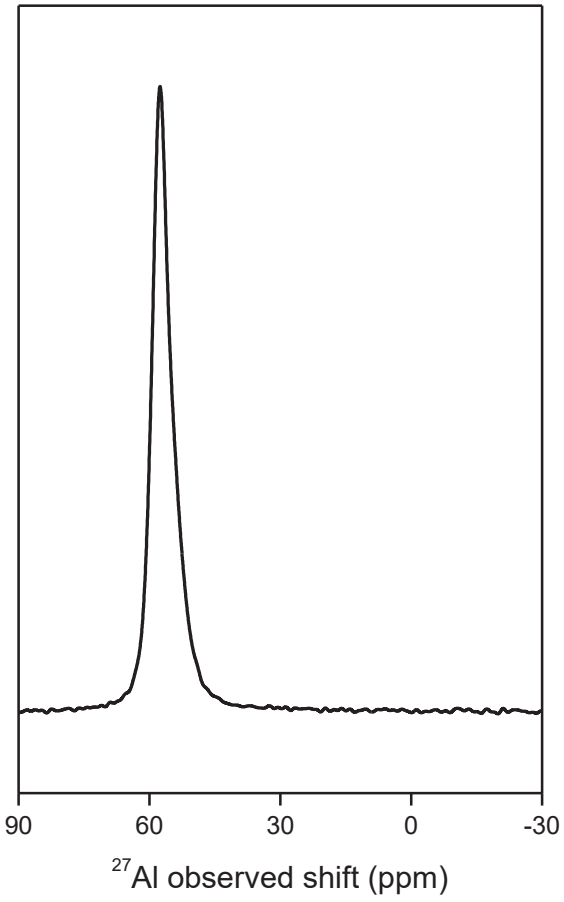


**Fig. 4.** $^{27}$Al MAS NMR spectrum of the as-made Al-rich *BEA zeolite.

silica surroundings – Si(4Si). The most intensive resonance at − 104.0 ppm, together with the signal at − 106.0 ppm were attributed to Si atoms neighboring 3 Si atoms and 1 Al atom – Si(3Si,1Al). Resonances below − 101 ppm usually indicate the presence of silanols – SiOH, yet in the case of Al-rich zeolites the signal characteristic for Si tetrahedra connected to 2 Si and 2 Al tetrahedra – Si(2Si,2Al) would be expected. In order to distinguish between those resonances a $^{29}$Si CP experiment was performed, which enhances the signal from Si atoms in the proximity of protons. As the result, the resonance at − 98.4 ppm was denoted as Si(2Si,2Al), and the remaining signals at − 100.5 and − 95.4 ppm were assigned to SiOH. As a matter of fact, the low intensity of the latter (SiOH) is in line with the well-crystalline structure and large crystals of the as-made *BEA zeolite suggested by XRD and SEM results.

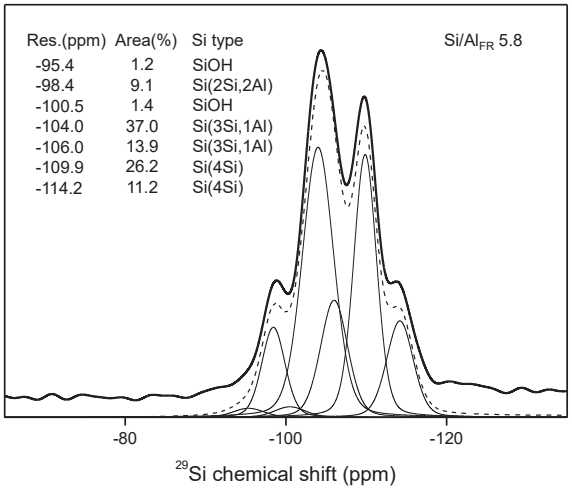


**Fig. 5.** $^{29}$Si MAS NMR spectrum of the as-made Al-rich *BEA zeolite (thick line) together with its fit (dashed line), and individual resonances (thin lines).

The correct assignment of the particular resonances allowed determining the framework Si/Al ratio ($Si/Al_{FR}$) equal 5.8 (for details see Experimental section). This value differs from the one obtained from the chemical analysis (Table 1) performed for the Co-exchanged sample (Si/Al 5.2), but still, the discrepancy is in the measures of method accuracy (below 10%). Moreover, signals at around − 100.5 and − 95.4 ppm can represent an overlap of the resonances of Si(2Si,2Al) and SiOH atoms. Based on the presented results, it can be concluded that the parent *BEA sample represents well-crystalline and low-defected zeolite with Al atoms present exclusively in the framework. Thus, the previously developed methodology involving the maximum exchange with Co(II) hexaaqua complex for studying Al distribution in Al-rich *BEA sample was performed [24].

The results of chemical analysis for the maximum loaded Co-*BEA sample are gathered in Table 1. The Co(II) ion-exchange capacity of the studied *BEA sample is equal to 0.48, thus close to the maximum theoretical value of 0.50 [24]. Nevertheless, for *BEA zeolites this value reflects the shares of both Al pairs and close Al atoms participating in the stabilization of Co(II) hexaaqua complexes in the hydrated form of the zeolite. However, only Al pairs with two Al atoms in one ring can compensate one bare Co(II) cation (or any other divalent transition metal ion) in dehydrated zeolite [24,46]. Therefore, distinguishing between Al pairs and close Al atoms is possible by using the results obtained from FTIR studies of dehydrated Co-sample. This allows quantification of bare Co(II) cations coordinated to Al pair forming cationic sites denoted as α, β, and γ [47]. Among them, the most populated cationic site for hosting divalent cations is the β site, arranged

in a 6-membered ring containing two Al atoms (Al pair) (Fig. 1a). Ligation of Co(II) by the framework Al atoms (of the Al pair) results in the perturbation of anti-symmetric T-O-T vibrations of the zeolitic lattice and is visible in the FTIR spectrum in the range of 990 – 840 $cm^{-1}$. The perturbation of anti-symmetric T-O-T vibrations enables the distinction of Co(II) location in cationic sites of the *BEA zeolite (see Supplementary material, Fig. S2). The concentration of Al pairs in obtained Al-rich *BEA sample was calculated according to Eq. 2 (Experimental section) and is equal to 0.74 mmol/g (30% of all Al atoms), while the fraction of close Al atoms (Eq. 3, Experimental section) reaches a value of 1.64 mmol/g (66% of all Al atoms). The population of Al pairs mainly occupying 6-membered rings of *BEA represents a sufficient starting point for the introduction of divalent iron cations, which might cooperate with each other as distant binuclear sites in the activation of molecular oxygen. The remaining fraction of 4% of all Al atoms (0.1 mmol/g) represents single Al atoms (Eq. 4 in the Experimental section, Table 1).

As shown above, Al-rich *BEA zeolite selected for the study possesses proper Al distribution with a high population of Al pairs enabling stabilization of bare divalent cations (Table 1). Such prepared Al-rich *BEA is a convenient material for the introduction of iron ions (Fe/Al 0.06) for further spectral investigation.

### 3.3. Mössbauer spectroscopy studies of the nature of iron species in Fe-*BEA

Mössbauer spectroscopy was used to determine the type of iron sites formed in Fe-*BEA (Al-rich) and the determination of iron centers involved in $O_2$ cleavage. The main advantage of Mössbauer spectroscopy is its ability to identify iron species, exclusively. For interpretation of the Mössbauer spectroscopy results of iron-zeolites, we generally accept the assignment presented in the following papers [3,10,42]. According to them all types of iron species present in studied samples can be detected and described by Mössbauer parameters: isomer shift (IS) and quadrupole splitting (QS) determining the oxidation state and symmetry of iron species, respectively. The presence of the doublet in the Mössbauer spectrum of iron zeolites with IS value higher than 0.7 mm/s confirmed the presence of Fe(II) centers. The value of IS below 0.5 mm/s characterized Fe(III) forms. The symmetry of Fe sites is characterized by the value of quadrupole splitting: QS $\geq$ 1.50 mm/s describing Oh-like symmetry and iron centers with QS $\leq$ 1.0 mm/s attributing to Td-like symmetry [42,48–50]. For the Mössbauer study, we intentionally selected Fe-*BEA (Al-rich) containing low iron loading Fe/Al 0.06, which guarantees the location of iron species as cationic sites exclusively. This approach allows studying both siting of iron centers and the behavior of particular sites in oxidation conditions. Mössbauer spectrum of Fe-*BEA (Al-rich) after 3 h evacuation at 450 °C together with its fit is presented in Fig. 6a. The spectral parameters obtained in the fitting process are gathered in Table 2. Mössbauer spectrum recorded under vacuum of evacuated Fe-*BEA was deconvoluted to three subspectra (goodness of the fit $\chi \sim 1$) with the value of IS indicating the exclusive presence of Fe(II) centers in studied Al-rich Fe-*BEA (no iron oxide

**Table 2**
Mössbauer parameters and spectral contribution of iron species in evacuated and treated with $O_2$ Al-rich $^{57}$Fe-*BEA.

| $^{57}$Fe-FER | | IS | QS | Rel. | Fe species |
|---|---|---|---|---|---|
| Fe/Al 0.06 | | mm/s | mm/s | % | |
| 3 h @ 450 °C | D1 | 0.81 | 1.09 | 24 | Fe(II) |
| | D2 | 1.20 | 2.10 | 18 | Fe(II) |
| | D3 | 0.80 | 0.60 | 58 | Fe(II) |
| + $O_2$ @ 220 °C | D4 | 0.37 | 2.70 | 6 | Fe(III) |
| | D5 | 0.90 | 2.70 | 35 | Fe(II) |
| | D6 | 0.41 | 1.00 | 59 | Fe(IV)=O |

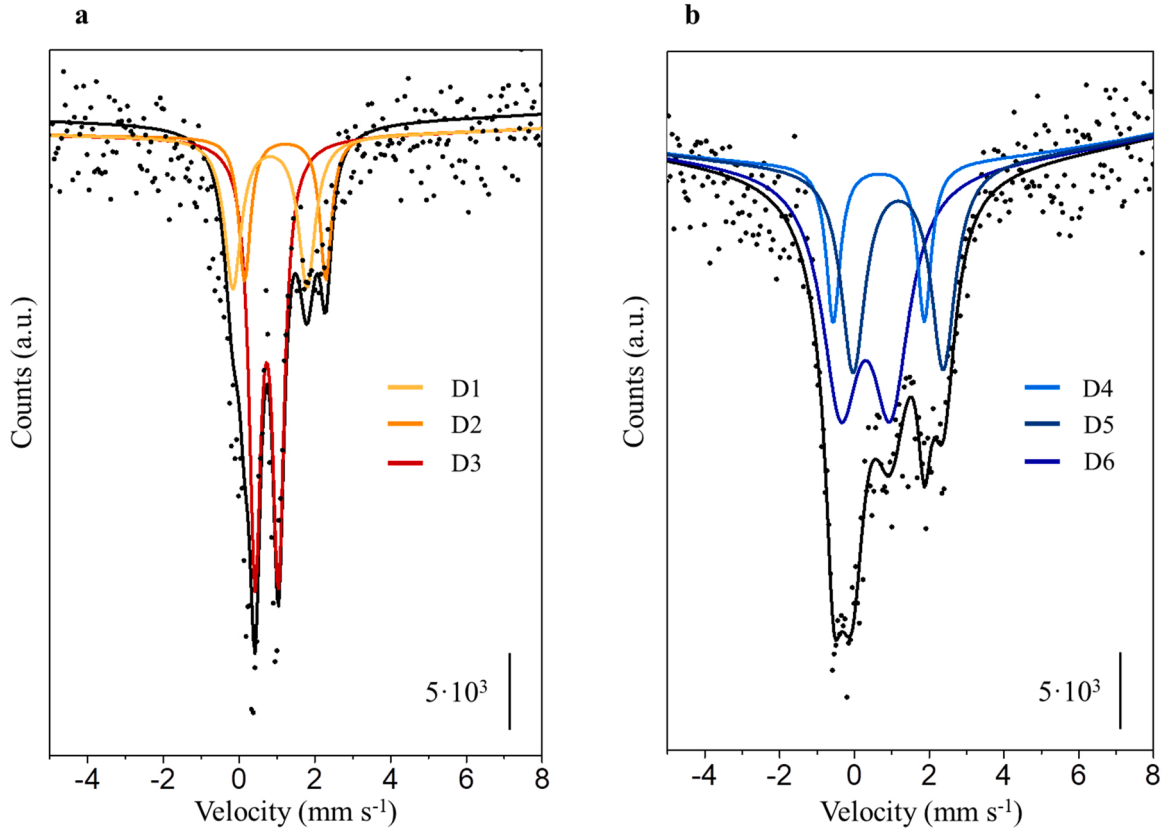


**Fig. 6.** Mössbauer spectra of $^{57}$Fe-*BEA (Al-rich) together with their fits recorded after the following treatments: 3 h evacuation at 450 °C under dynamic vacuum (a), 3 h evacuation at 450 °C for 3 h, then interaction with $O_2$ (101352 Pa) for 60 min at 220 °C and after that $O_2$ desorption at 220 °C for 5 min (b).

present, see Supplementary material, Fig. S3.). The parameters of doublets D1 and D3 are typical for Fe(II) Td-like coordination. This type of species was previously assigned to bare Fe(II) stabilized in zeolite rings containing two Al atoms. The low value of QS indicates that the symmetry of Fe(II) described by the D1 and D3 doublet is close to Td coordination. Similar values of the parameters obtained for FER or ZSM-5 were assigned to Fe(II) in β cationic positions [3,28,48–51]. However, in Fe-*BEA Al-rich the value of the QS component describing Fe(II) in β cationic site has a higher value in contrast to those observed in Fe-FER or Fe-ZSM-5. This suggests the lower symmetry of Fe(II) in the β position in *BEA. This observation is in agreement with DFT calculations, which revealed that Fe(II) in β is withdrawn above the zeolite ring (Fig. 1), in contrast to Fe-FER and Fe-ZSM-5, in which Fe(II) is in a planar position. Based on the literature data the doublet D2 was pointed out to Fe(II) located in α cationic positions. The higher value of QS indicates the symmetry of Fe(II) close to Oh–like. In the investigated Fe-*BEA, divalent iron occupied mainly β cationic positions of the zeolite lattice (88%), the rest of the iron is located in α cationic positions (component D2).

Mössbauer spectrum recorded at RT after interactions with $O_2$ at 220 °C is presented in Fig. 6b. Results of spectra deconvolutions (Table 2) reveal that after interactions with $O_2$ majority (65%) of divalent iron species present in the evacuated Fe-*BEA (Al-rich) was oxidized. The new components (D4 and D6) with IS values lower than 0.5 mm/s can be assigned to the oxidized form of iron. Low populated (6% of total Fe) D4 with a high value of QS (QS= 2.70 mm/s) can be attributed to isolated Fe(III) in Oh-like coordination. The presence of this type of species was observed previously in silica-rich Fe-FER, Fe-ZSM-5, and Fe-*BEA treated in an oxidizing atmosphere. The major faction (59% of the total Fe) of the spectrum represents a new component D6 with IS = 0.41 and QS = 1.00 mm/s. The value of IS indicates that iron is present in a higher-than-divalent oxidation state and the value of QS specifies the coordination close to Td. The component D6 exhibiting similar values of Mössbauer parameters was detected in Mössbauer spectra of Fe-zeolites (silica-rich FER, ZSM-5, and *BEA) after interaction with $N_2O$ or very recently with $O_2$ (Fe-FER). The authors assigned this component to the active oxygen form originating from $N_2O$ or $O_2$ splitting, which is stabilized on iron ($[Fe(IV){=}O^{2-}]^{2+}$. It was shown that this type of species exhibits a high oxidation potential towards methane to methanol and benzene to phenol transformation [3,10]. The value of Mössbauer parameters characterizing ions with stabilized active oxygen subtle differs depending on the zeolite topology, which controls the geometry of iron sites. However, it is commonly accepted that Fe sites able to stabilize active oxygen form have to be embedded in the zeolite matrix as bare cations and stabilized in the zeolite ring containing two Al atoms [24]. It confirms that the position of iron bare cations is defined by the structure of the zeolite and Al distribution. These two factors explain the changes in the value of Mössbauer parameters depending on the zeolite matrix. Mössbauer parameters of subspectrum D5 are typical for Fe(II). This species represents the fraction of iron that resisted $O_2$ oxidation.

### 3.4. X-ray absorption studies of the Fe-*BEA redox behavior

The behavior of the iron species present in the zeolite under each reaction step i.e. (i) activation in He, (ii) oxidation by $O_2$, and (iii) methane oxidation was additionally followed using in-situ XANES, which allows getting more insight into the oxidation state and geometry of the active center. The XANES spectra (Fig. 7) consist of pre-edge and absorption edge region, which are sensitive to both oxidation state and coordination geometry. The XANES spectra recorded for the ex-situ sample, prior to any treatment, are shown in Fig. S4. The position of the edge, which is similar to the $Fe_2O_3$ (Fig. S4), and the low intensity of the pre-edge, point towards Fe(III) species in an octahedral geometry, respectively [52]. During the activation procedure (Fig. S3) pronounced changes occur i.e. (i) shift of absorption edge towards lower energies and

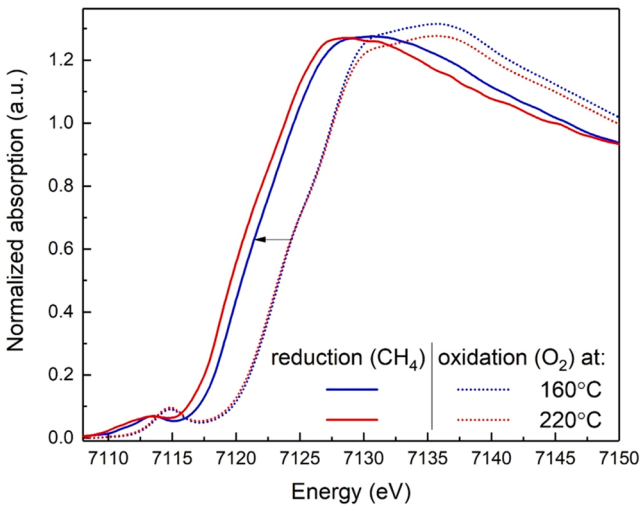


**Fig. 7.** In-situ transmission Fe K-edge XANES spectra of Fe-*BEA recorded at 160 ℃ and 220 ℃ under a stream of $O_2$ (dotted line) or $CH_4$ (straight line).

(ii) replacement of the pre-edge feature at ca. 7114.8 eV by a new one at ca. 7113.4 eV, both suggesting a partial reduction of Fe(III) to Fe(II). The discrepancy between XANES and Mössbauer, which suggests that all iron species are in the reduced form, may arise from possible different redox behavior of the $^{57}Fe$ as well as different conditions during activation (vacuum vs. flow).

The XANES spectra recorded after exposure of the activated material to the $O_2$ atmosphere at 160 ℃ and 220 ℃ are shown in Fig. 7. The XANES spectra acquired after the addition of $O_2$ underwent pronounced changes. During activation, part of the species were reduced from Fe(III) to Fe(II). Those species were later on fully oxidized by $O_2$ to Fe(III) species, which is identified by (i) the similar position of the absorption edge to the $Fe_2O_3$ reference (Fig. S5) and (ii) arising pre-edge feature at ca. 7114.8 eV. The XANES features observed for this material under $O_2$ are very similar to the reported by Westre et al. for Fe(salen)Cl in square-pyramidal geometry and for Fe-ZSM-5 catalyst in our previous studies [53,54].

The oxidation of the material under the $O_2$ atmosphere was followed by the introduction of $CH_4$, the XANES spectra recorded after equilibration are shown in Fig. 7 at 160 ℃ and 220 ℃. XANES spectra recorded under the $O_2$ atmosphere were added in order to follow the changes occurring. The introduction of $CH_4$ resulted in a reduction of Fe (III) species to Fe(II), which is represented by (i) the replacement of the pre-edge feature at ca. 7114.8 eV by one at ca. 7113.4 eV and (ii) a significant shift of the absorption edge towards lower energies by ca. 3.7 eV. The absorption edge position of the spectra obtained under $CH_4$ at 220 ℃ matches that of the $Fe_2O_3$ reference (Fig. S5), which suggests that all of the species may shuffle between Fe(III) and Fe(II) and are involved in the redox cycle at 220 ℃. Compared to the spectra recorded for Fe-ZSM-5 in our previous work the one acquired under a reducing atmosphere for Fe-*BEA does not show a shoulder at the absorption edge at ca. 7121 eV, which is a 1 s → 4p transition and is a fingerprint of Fe species in square planar geometry. This is in agreement with the results acquired by Mössbauer, which suggest that Fe(II) species present in *BEA zeolite after activation show low symmetry, indicating that iron is pulled out of square planar geometry and would explain the lack of such shoulder.

On the other hand, XANES spectra recorded at 160 ℃ under $CH_4$ suggest that a part of iron species remained oxidized as suggested by a smaller shift of the absorption edge (of ca. 3.2 eV towards lower energies) compared to 220 ℃. In order to determine the oxidation state linear combination fitting was applied using the spectra recorded under the most oxidizing and reducing atmosphere. The obtained results suggest that 77.2% of Fe(III) species present were reduced to Fe(II) under

$CH_4$ at 160 ℃. The best fitting parameters of EXAFS are reported in Table S1 (Supplementary materials, Fig. S6). The obtained results suggest two oxygen sub-shell with average Fe-O distances of 1.73 and 2.00 Å with CN = 0.8 and 4.3, respectively. After the introduction of $CH_4$, fitting the first shell at ca. 1.73 Å was not possible, which is most likely related to the consumption of the formed α-O.

### 3.5. Detection and identification of oxidation products

The results obtained from Mössbauer and XAS spectroscopies confirmed that after evacuation at 450 °C, the Al-rich Fe-*BEA sample consists of a predominant fraction of Fe(II) located in cationic positions. Small discrepancies between Mössbauer and XAS results obtained for samples after the dehydration might be connected with the different methodology of this step (dynamic vacuum vs. inert gas flow) and application of the different sample, which for Mössbauer studies was prepared separately with enriched $^{57}$Fe-source (see Experimental section). A part of Fe(II) centers can form sites that exhibit strong redox behavior towards $O_2$ activation and subsequent reduction by $CH_4$. The iron centers previously oxidized by $O_2$, after their interaction with $CH_4$, exhibit the same symmetry and oxidation state, as was observed in evacuated samples (Figs. 6, 7 and Table 2), which confirms that the redox process took place, and the products of the reaction were released form the active iron centers. Suggested by the results of X-ray absorption spectroscopy spontaneous release of the products of methane oxidation from binuclear iron centers in Al-rich *BEA was further studied with the use of FTIR spectroscopy and mass spectrometry by analyzing the outlet gasses. The latter was also employed for their quantitative analysis. Note, that during the reactivity tests, chosen sample with low iron loading (Fe/Al 0.05) and the reaction conditions (220 °C) were in line with those applied during the spectroscopic studies of the iron centers and targeted on the highest possible release of the oxidation products, not maximum productivity to any of the oxygenates.

The FTIR spectrum of the volatile products of the interaction between the active oxygen stabilized on iron centers in Al-rich *BEA with methane at 220 °C is depicted in Fig. 8a. The spectrum contains two bands at 2925 and 2850 $cm^{-1}$, which are characteristic for the vibrations of methoxy species. The presence of these bands clearly indicates the formation of methanol [55]. In addition, the bands at 2360 and 2335 $cm^{-1}$ typical for the $CO_2$ stretching vibrations are visible in the acquired spectrum. Moreover, the band at 3215 $cm^{-1}$ was found in the region of OH vibrations confirming water as one of the reaction products. The presence of both $CO_2$ and $H_2O$ among the reaction products suggests total oxidation of $CH_4$. Similar conclusions were driven based on the FTIR products analysis performed in the work of Sushkevich et al., in which both carbon monoxide and carbon dioxide were found after a methane oxidation reaction over Cu-MOR [56]. Finally, a blank FTIR experiment without the $O_2$ oxidation step was performed at 220 °C, see Fig. 8b, which revealed only a weak signal from $CO_2$, and no signal originating from oxygen-containing compounds, which confirms that the $O_2$ activation of iron centers in Al-rich *BEA is an essential step for the further oxidation process.

In order to quantify products of $CH_4$ oxidation by α-oxygen formed over Al-rich Fe-*BEA, and the stability of the catalytic system, the activity tests with mass spectrometry detection of the reaction products were performed at 220 °C in three consecutive redox cycles. The Fe-*BEA (Al-rich) was activated at 450 °C, cooled down to 220 °C and at this temperature oxidized by $O_2$, and subsequently, interacted with $CH_4$ (for details see the Experimental section). The mass spectra of such three redox cycles (Fig. 9) revealed the formation of two main reaction products attributed to signals with $m/z = 31$ (methanol) and $m/z = 44$ (carbon dioxide).

Quantitative analysis of the mass spectra undoubtedly confirms the oxidation of methane over $O_2$ activated Al-rich Fe-*BEA sample with carbon dioxide as a main product under the reaction conditions (see SI Table S2). The methanol production over Al-rich Fe-*BEA obtained at 220 °C (Fig. 9) varied in three subsequent redox cycles from 0.30 to 0.45 μmol/$g_{cat}$. A significant increase (four times) of $CO_2$ productivity in the third cycle in comparison to the first one suggests a higher tendency of the redox system towards total oxidation of $CH_4$ or over-oxidation of previously formed methanol. However, the productivity of methanol over Fe-*BEA increased in three cycles of oxidation with $O_2$ and interaction with methane carried at 220 °C. This phenomenon might be connected with the evolution of the transition metal ion active sites during the ongoing reaction, which leads to the enrichment of the fraction of Fe(II) in β cationic positions and thus an increase in the number of binuclear Fe(II) centers being responsible for $O_2$ splitting and methane oxidation in the studied system.[57] The latter statement is confirmed by a strong decrease (around 50%) in the system productivity of methanol in comparison with $CO_2$. It has to be noted that presented quantitative results were obtained for Fe-*BEA sample with low iron loading (Fe/Al 0.05) convenient for spectral studies but not

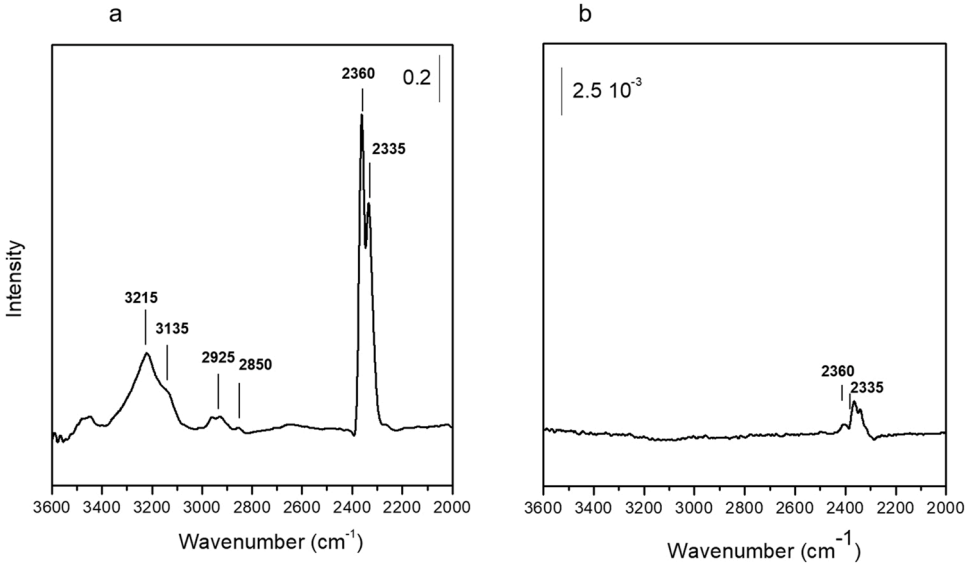


**Fig. 8.** FTIR spectra of the gas phase acquired during the reaction of Al-rich Fe-*BEA with $O_2$ and methane (a), and interaction of methane with Al-rich Fe-*BEA without previous treatment of the sample with $O_2$ (blank experiment) (b).

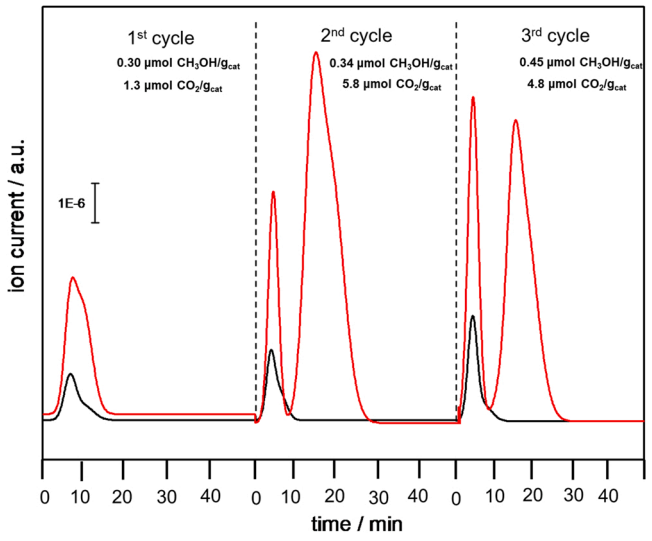


**Fig. 9.** Time dependence of the signals with $m/z = 31$ and 44 related to methanol and carbon dioxide forming over Fe-*BEA after $O_2/CH_4$ interaction at 220 °C monitored by mass spectrometry in three consecutive redox cycles. The numbers in the right corner represent the productivity of the detected oxidation products (see Supplementary material).

guaranteeing the highest catalytic performance. Moreover, carrying out the reaction at an elevated temperature (220 °C) can facilitate the recombination of α-oxygen stabilized over binuclear iron sites in Al-rich *BEA leading to lower productivity of the oxygenates [28]. However, the oxidation of methane was used solely as a testing reaction to confirm the formation of α-O, so the presence of binuclear iron centers in the studied sample. Moreover, the presence of the oxygenates ($CO_2$ and $CH_3OH$) was confirmed also in three redox cycles ($O_2/CH_4$) carried at ambient conditions (50 °C) and subsequent temperature programmed desorption exhibited only increasing of the signal $m/z$ 18 attributed to $H_2O$ (see Supplementary material, Fig. S9 and S10).

The results of FTIR and mass spectrometry analysis of outlet gasses confirmed the ability of Al-rich Fe-*BEA pretreated with molecular oxygen to oxidize $CH_4$ with the formation of $CO_2$ and methanol. This particular reaction was chosen as a test reaction, confirming the engagement of a very active α-O species in the formation of oxygenates. Obtained results constitute an important voice in the discussion present in the literature related to the mechanism of products' formation and desorption in methane oxidation by α-O. The interaction of methane with α-O originating from $N_2O$ assumes the formation of methoxy species bound to the iron sites in the zeolite matrix, and was confirmed experimentally by FTIR spectral study [58]. The appearance of methanol, in this case, occurred by protonation of the methoxy intermediates by the water molecules, which allows methanol desorption to the gas phase at a temperature higher than 250 °C. However, recently it was shown that the structure of the zeolitic framework significantly influences the desorption of the methane oxidation products [11]. Theoretical studies revealed that in zeolites with transport restrictions (cavities with iron active sites interconnected by 8-membered rings) e.g. chabasite (CHA) or ferrierite (FER), methane oxidation by α-O (from $N_2O$) occurred via rebound mechanism [21]. In this mechanism, methyl radical appears after the abstraction of a proton from methane by α-O, and Fe-OH is formed. Subsequently, methyl radical attacks the same iron site producing a methanol molecule which is released to the gas phase. Desorption of methanol as a product of methane oxidation by α-O originating from both $N_2O$ and $O_2$ over Fe-FER was already experimentally confirmed [28,29]. However, unlike in the case of narrow-pored zeolites, DFT calculations suggested that the spontaneous release of methane oxidation products is limited over wide-pore zeolitic topologies with 10-membered ring or 12-membered rings channels (MFI or *BEA respectively) [11]. Yet, the results reported in this study clearly evidence, that methanol can be formed and released to the gas phase also in the case of wide-pore *BEA zeolite.

## 4. Conclusions

The results presented in this work confirmed that low-defected Al-rich *BEA material with a high population of Al pairs, additionally prepared by eco-friendly, template-free synthesis protocol, allowed hosting distant binuclear iron centers. Moreover, extensive spectroscopic studies provide the first experimental evidence of molecular oxygen activation by its cleavage over binuclear iron centers in zeolite of topology other than FER. The results of both Mössbauer and X-ray absorption spectroscopies unanimously confirmed that molecular oxygen interacts with iron centers in Al-rich *BEA with the formation of active oxygen form called α-oxygen, which exhibits unique oxidation potential towards the attack on inert C-H bond of $CH_4$ molecule, resulting in the formation of oxygenates already at ambient temperatures. Furthermore, in-situ studies revealed that methane treatment of oxidized samples leads to the full reduction of Fe(III) to bare Fe(II) species, indicating the removal of the reaction products from active centers. In-situ FTIR and mass spectrometry evidenced the spontaneous release of carbon dioxide and methanol in the gas stream. Thus, the confirmation of the presence of methane oxidation products is the unambiguous evidence of the formation of α-oxygen species over binuclear iron centers in the *BEA topology. Additionally, this finding supports previous DFT predictions on the diffusion mechanism of methane oxidation products from wide-pored zeolitic topologies. Based on the results presented in this contribution, it can be stated, that distant binuclear iron centers are not unique for the FER topology, and can be prepared in other zeolitic matrices when the structural requirements to the site arrangement as well as Al distribution in the matrix are met. This is essential both for the development of catalysts for selective oxidation of methane, and for highly desired from an energetic point of view oxidation processes involving long-chained hydrocarbons. It is due to enhance of the transport properties in wide-pore *BEA zeolite topology. Moreover, in the case of the application of successfully prepared Al-rich zeolites, the formation of a high fraction of distant binuclear TMI centers being the active sites in oxidation reaction is feasible.

## CRediT authorship contribution statement

**Agnieszka Kornas** – activity tests (MS, FTIR), XAS measurements, Data curation, Visualization, Conceptualization, **Edyta Tabor** – Conceptualization, Mössbauer studies, XAS measurements, FTIR spectra interpretation, Sample preparation, Manuscript preparation, **Dominik K. Wierzbicki** – XAS data analysis and interpretation, Manuscript preparation, **Joanna E. Olszowka** – NMR study, FTIR study for determination of Al distribution, Sample preparation, Manuscript preparation, **Radim Pilar** – synthesis and structural characterization of the sample, **Jiri Dedecek** – Conceptualization, NMR study, Al distribution, Manuscript preparation, **Michal Sliwa** – Activity tests, **Hana Jirglova** – FTIR study, **Stepan Sklenak** – DFT calculations, Visualization, Manuscript preparation, **Dorota Rutkowska-Zbik** - Manuscript preparation, **Kinga Mlekodaj** – Conceptualization, Determination of Al-distribution, activity tests (FTIR, MS), XAS measurements, Manuscript preparation.

## Declaration of Competing Interest

The authors declare that they have no known competing financial interests or personal relationships that could have appeared to influence the work reported in this paper.

## Data availability

Data will be made available on request.

## Acknowledgments

This work was supported by the Grant Agency of the Czech Republic under project # 19–02901 S, 21–45567 L, and project RVO: 61388955nd. This work was supported by the Ministry of Education, Youth and Sports of the Czech Republic through the e-INFRA CZ (ID:90140). Chemical analysis was provided in the frame of CATPRO (Ministry of Education, Youth and Sports, ref. no. MSMT-1000/2016, under Project No. LM2015039), which has been integrated into the National Program for Sustainability I of the Ministry of Education, Youth and Sports of the Czech Republic through the project Development of the UniCRE Centre, Project Code LO1606. This research was funded in part by the National Science Centre, Poland grant no. 2020/39/I/ST4/02559. For the purpose of Open Access, the author has applied a CC-BY public copyright licence to any Author Accepted Manuscript (AAM) version arising from this submission.

We acknowledge the Paul Scherrer Institute, Villigen, Switzerland for provision of synchrotron radiation beamtime at the SuperXAS beamline.

## Appendix A. Supporting information

Supplementary data associated with this article can be found in the online version at doi:10.1016/j.apcatb.2023.122915.

## References

[1] P.J. Smeets, J.S. Woertink, B.F. Sels, E.I. Solomon, R.A. Schoonheydt, Transition-metal ions in zeolites: coordination and activation of oxygen, Inorg. Chem. 49 (2010) 3573–3583, https://doi.org/10.1021/ic901814f.

[2] H.M. Rhoda, A.J. Heyer, B.E.R. Snyder, D. Plessers, M.L. Bols, R.A. Schoonheydt, B. F. Sels, E.I. Solomon, Second-Sphere Lattice Effects in Copper and Iron Zeolite Catalysis, Chem. Rev., doi:10.1021/acs.chemrev.1c00915.

[3] B.E.R. Snyder, P. Vanelderen, M.L. Bols, S.D. Hallaert, L.H. Bottger, L. Ungur, K. Pierloot, R.A. Schoonheydt, B.F. Sels, E.I. Solomon, The active site of low-temperature methane hydroxylation in iron-containing zeolites, 317-+, Nature 536 (2016) https://doi.org/10.1038/nature19059.

[4] B.E.R. Snyder, M.L. Bols, R.A. Schoonheydt, B.F. Sels, E.I. Solomon, Iron and copper active sites in zeolites and their correlation to metalloenzymes, Chem. Rev. 118 (2018) 2718–2768, https://doi.org/10.1021/acs.chemrev.7b00344.

[5] E.I. Solomon, A. Jose, Spiers Memorial Lecture: activating metal sites for biological electron transfer, Faraday Discuss. 234 (2022) 9–30, https://doi.org/10.1039/d2fd00001f.

[6] S. Sirajuddin, A.C. Rosenzweig, Enzymatic oxidation of methane, Biochem 54 (2015) 2283–2294, https://doi.org/10.1021/acs.biochem.5b00198.

[7] R.B. Jackson, E.I. Solomon, J.G. Canadell, M. Cargnello, C.B. Field, Methane removal and atmospheric restoration, Nat. Sustain 2 (2019) 436–438, https://doi.org/10.1038/s41893-019-0299-x.

[8] L.L. Sun, Y. Wang, N.J. Guan, L.D. Li, Methane Activation and Utilization: Current Status and Future Challenges, Energy Technol., 8 (2020), doi:Unsp 190082610.1002/ente.201900826.

[9] Q. Zhang, J.H. Yu, A. Corma, Applications of Zeolites to C1 Chemistry: Recent Advances, Challenges, and Opportunities, Adv. Mater., 32 (2020), doi: 200292710.1002/adma.202002927.

[10] M.L. Bols, S.D. Hallaert, B.E.R. Snyder, J. Devos, D. Plessers, H.M. Rhoda, M. Dusselier, R.A. Schoonheydt, K. Pierloot, E.I. Solomon, B.F. Sels, Spectroscopic Identification of the alpha-Fe/alpha-O Active Site in Fe-CHA Zeolite for the Low-Temperature Activation of the Methane C-H Bond, J. Am. Chem. Soc. 140 (2018) 12021–12032, https://doi.org/10.1021/jacs.8b05877.

[11] M.L. Bols, H.M. Rhoda, B.E.R. Snyder, E.I. Solomon, K. Pierloot, R.A. Schoonheydt, B.F. Sels, Advances in the synthesis, characterisation, and mechanistic understanding of active sites in Fezeolites for redox catalysts, Dalton Trans. 49 (2020) 14749–14757, https://doi.org/10.1039/d0dt01857k.

[12] M.L. Bols, B.E.R. Snyder, H.M. Rhoda, P. Cnudde, G. Fayad, R.A. Schoonheydt, V. Van Speybroeck, E.I. Solomon, B.F. Sels, Coordination and activation of nitrous oxide by iron zeolites, Nat. Catal. 4 (2021) 332–340, https://doi.org/10.1038/s41929-021-00602-4.

[13] P. Vanelderen, B.E.R. Snyder, M.L. Tsai, R.G. Hadt, J. Vancauwenbergh, O. Coussens, R.A. Schoonheydt, B.F. Sels, E.I. Solomon, Spectroscopic definition of the copper active sites in mordenite: selective methane oxidation, J. Am. Chem. Soc. 137 (2015) 6383–6392, https://doi.org/10.1021/jacs.5b02817.

[14] G. Zhao, A. Adesina, E. Kennedy, M. Stockenhuber, Formation of Surface Oxygen Species and the Conversion of Methane to Value-Added Products with N2O as Oxidant over Fe-Ferrierite Catalysts, ACS Catal. 10 (2020) 1406–1416, https://doi.org/10.1021/acscatal.9b03466.

[15] G. Zhao, K. Chodyko, E. Benhelal, A. Adesina, E. Kennedy, M. Stockenhuber, Methane oxidation by N2O over Fe-FER catalysts prepared by different methods: Nature of active iron species, stability of surface oxygen species and selectivity to products, J. Catal. 400 (2021) 10–19, https://doi.org/10.1016/j.jcat.2021.04.019.

[16] G. Zhao, P. Yan, K. Procter, A. Adesina, Y. Jin, E. Kennedy, M. Stockenhuber, Effect of desilication on the catalytic activity of Fe-FER for direct, selective, partial oxidation of methane, J. Catal. 417 (2023) 140–152, https://doi.org/10.1016/j.jcat.2022.11.030.

[17] K. Mlekodaj, M. Lemishka, S. Sklenak, J. Dedecek, E. Tabor, Dioxygen splitting at room temperature over distant binuclear transition metal centers in zeolites for direct oxidation of methane to methanol, Chem. Comm. 57 (2021) 3472–3475, https://doi.org/10.1039/d1cc00909e.

[18] E. Tabor, M. Lemishka, J.E. Olszowka, K. Mlekodaj, J. Dedecek, P. C. Andrikopoulos, S. Sklenak, Splitting Dioxygen over Distant Binuclear Fe Sites in Zeolites. Effect of the Local Arrangement and Framework Topology, ACS Catal. 11 (2021) 2340–2355, https://doi.org/10.1021/acscatal.0c04459.

[19] E. Tabor, J. Dedecek, K. Mlekodaj, Z. Sobalik, P.C. Andrikopoulos, S. Sklenak, Dioxygen dissociation over man-made system at room temperature to form the active α-oxygen for methane oxidation, eaaz9776, Sci. Adv. 6 (2020), https://doi.org/10.1126/sciadv.aaz9776.

[20] E. Tabor, M. Lemishka, Z. Sobalik, K. Mlekodaj, P.C. Andrikopoulos, J. Dedecek, S. Sklenak, Low-temperature selective oxidation of methane over distant binuclear cationic centers in zeolites, Commun. Chem. 2 (2019) 71, https://doi.org/10.1038/s42004-019-0173-9.

[21] F. Goltl, C. Michel, P.C. Andrikopoulos, A.M. Love, J. Hafner, I. Hermans, P. Sautet, Computationally Exploring Confinement Effects in the Methane-to-Methanol Conversion Over Iron-Oxo Centers in Zeolites, ACS Catal. 6 (2016) 8404–8409, https://doi.org/10.1021/acscatal.6b02640.

[22] Z.R. Jovanovic, J.P. Lange, M. Ravi, A.J. Knorpp, V.L. Sushkevich, M.A. Newton, D. Palagin, J.A. van Bokhoven, Oxidation of methane to methanol over Cu-exchanged zeolites: Scientia gratia scientiae or paradigm shift in natural gas valorization? J. Catal. 385 (2020) 238–245, https://doi.org/10.1016/j.jcat.2020.02.001.

[23] J. Meyet, K. Searles, M.A. Newton, M. Worle, A.P. van Bavel, A.D. Horton, J.A. van Bokhoven, C. Coperet, Monomeric Copper(II) Sites Supported on Alumina Selectively Convert Methane to Methanol, Angew. Chem. Int. Ed. 58 (2019) 9841–9845, https://doi.org/10.1002/anie.201903802.

[24] J. Dedecek, E. Tabor, S. Sklenak, Tuning the aluminum distribution in zeolites to increase their performance in acid-catalyzed reactions, ChemSusChem 12 (2019) 556–576, https://doi.org/10.1002/cssc.201801959.

[25] P. Sazama, E. Tabor, P. Klein, B. Wichterlova, S. Sklenak, L. Mokrzycki, V. Pashkkova, M. Ogura, J. Dedecek, Al-rich beta zeolites. Distribution of Al atoms in the framework and related protonic and metal-ion species, J. Catal. 333 (2016) 102–114, https://doi.org/10.1016/j.jcat.2015.10.010.

[26] P. Sazama, D. Kaucky, J. Moravkova, R. Pilar, P. Klein, J. Pastvova, E. Tabor, S. Sklenak, I. Jakubec, L. Mokrzycki, Superior activity of non-interacting close acidic protons in Al-rich Pt/H-*BEA zeolite in isomerization of n-hexane, Appl. Catal. A: Gen. 533 (2017) 28–37, https://doi.org/10.1016/j.apcata.2016.12.016.

[27] K. Mlekodaj, M. Lemishka, S. Sklenak, J. Dedecek, E. Tabor, Dioxygen splitting at room temperature over distant binuclear transition metal centers in zeolites for direct oxidation of methane to methanol, Chem. Commun. (2021), https://doi.org/10.1039/d1cc00909e.

[28] E. Tabor, J. Dedecek, K. Mlekodaj, Z. Sobalik, P.C. Andrikopoulos, S. Sklenak, Dioxygen dissociation over man-made system at room temperature to form the active alpha-oxygen for methane oxidation, Sci. Adv. 6 (2020) eaaz977610.1126/sciadv.aaz9776.

[29] E. Tabor, M. Lemishka, Z. Sobalik, K. Mlekodaj, P.C. Andrikopoulos, J. Dedecek, S. Sklenak, Low-temperature selective oxidation of methane over distant binuclear cationic centers in zeolites, Commun. Chem. 2 (2019), 71 10.1038/s42004-019-0173-9.

[30] K. Mlekodaj, J.E. Olszowka, V. Tokarova, E. Tabor, A. Kasparek, J. Novakova, G. Stavova, O. Gonsiorova, L. Peliskova, J. Brus, R. Pilar, P. Klein, J. Dedecek, Effect of alkali-free synthesis and post-synthetic treatment on acid sites in beta, Zeolites, Mol. 25 (2020), 3434 10.3390/molecules25153434.

[31] R. Pilar, J. Moravkova, G. Sadovska, S. Sklenak, L. Brabec, J. Pastvova, P. Sazama, Controlling the competitive growth of zeolite phases without using an organic structure-directing agent. Synthesis of Al-rich *BEA, Microporous Mesoporous Mater. 333 (2022), 111726 10.1016/j.micromeso.2022.111726.

[32] S. Sklenak, P.C. Andrikopoulos, B. Boekfa, B. Jansang, J. Novakova, L. Benco, T. Bucko, J. Hafner, J. Dedecek, Z. Sobalik, N2O decomposition over Fe-zeolites: Structure of the active sites and the origin of the distinct reactivity of Fe-ferrierite, Fe-ZSM-5, and Fe-beta. A combined periodic DFT and multispectral study, J. Catal. 272 (2010) 262–274, https://doi.org/10.1016/j.jcat.2010.04.008.

[33] K. Jisa, J. Novakova, M. Schwarze, A. Vondrova, S. Sklenak, Z. Sobalik, Role of the Fe-zeolite structure and iron state in the N2O decomposition: Comparison of Fe-FER, Fe-BEA, and Fe-MFI catalysts, J. Catal. 262 (2009) 27–34, https://doi.org/10.1016/j.jcat.2008.11.025.

[34] Z. Sobalik, E. Tabor, J. Novakova, N.K. Sathu, K. Zaveta, Role of active oxygen and NOx species in N2O decomposition over Fe-ferrierite, J. Catal. 289 (2012) 164–170, https://doi.org/10.1016/j.jcat.2012.02.007.

[35] G. Engelhardt, U. Lohse, E. Lippmaa, M. Tarmak, M. Magi, SI-29NMR investigation of silicon-aluminum ordering in the aluminosilicate framework of faujasite-type zeolites, Z. Anorg. Allg. Chem. 482 (1981) 49–64, https://doi.org/10.1002/zaac.19814821106.

[36] C.A. Fyfe, Y. Feng, H. Grondey, G.T. Kokotailo, H. Gies, One- and two-dimensional high-resolution solid-state NMR studies of zeolite lattice structures, Chem. Rev. 91 (1991) 1525–1543, https://doi.org/10.1021/cr00007a013.

[37] J. Dedecek, Z. Sobalik, B. Wichterlova, Siting and distribution of framework aluminium atoms in silicon-rich zeolites and impact on catalysis, Catal. Rev. -Sci. Eng. 54 (2012) 135–223, https://doi.org/10.1080/01614940.2012.632662.
[38] J. Dědeček, D. Kaucký, B. Wichterlová, O. Gonsiorová, Co2+ ions as probes of Al distribution in the framework of zeolites. ZSM-5 study, Phys. Chem. Chem. Phys. 4 (2002) 5406–5413, https://doi.org/10.1039/b203966b.
[39] A.A. Gabrienko, I.G. Danilova, S.S. Arzumanov, L.V. Pirutko, D. Freude, A. G. Stepanov, Direct measurement of zeolite brønsted acidity by FTIR spectroscopy: solid-state 1H MAS NMR approach for reliable determination of the integrated molar absorption coefficients, J. Phys. Chem. C. 122 (2018) 25386–25395, https://doi.org/10.1021/acs.jpcc.8b07429.
[40] L. Čapek, J. Dědeček, B. Wichterlová, Co-beta zeolite highly active in propane–SCR-NOx in the presence of water vapor: effect of zeolite preparation and Al distribution in the framework, J. Catal. 227 (2004) 352–366, https://doi.org/10.1016/j.jcat.2004.08.001.
[41] J. Dedecek, L. Capek, D. Kaucky, Z. Sobalik, B. Wichterlova, Siting and distribution of the Co ions in beta zeolite: A UV-Vis-NIR and FTIR study, J. Catal. 211 (2002) 198–207, https://doi.org/10.1006/jcat.2002.3697.
[42] P. Sazama, J. Moravkova, S. Sklenak, A. Vondrov, E. Tabor, G. Sadovska, R. Pilar, Effect of the Nuclearity and Coordination of Cu and Fe Sites in beta Zeolites on the Oxidation of Hydrocarbons, ACS Catal. 10 (2020) 3984–4002, https://doi.org/10.1021/acscatal.9b05431.
[43] A.H. Clark, J. Imbao, R. Frahm, M. Nachtegaal, ProQEXAFS: a highly optimized parallelized rapid processing software for QEXAFS data, J. Synchrotron Radiat. 27 (2020) 551–557, https://doi.org/10.1107/s1600577519017053.
[44] B. Ravel, M. Newville, ATHENA, ARTEMIS, HEPHAESTUS: data analysis for X-ray absorption spectroscopy using IFEFFIT, J. Synchrotron Radiat. 12 (2005) 537–541, https://doi.org/10.1107/s0909049505012719.
[45] M. Ogura, K. Itabashi, J. Dedecek, T. Onkawa, Y. Shimada, K. Kawakami, K. Onodera, S. Nakamura, T. Okubo, Stabilization of bare divalent Fe(II) cations in Al-rich beta zeolites for superior NO adsorption, J. Catal. 315 (2014) 1–5, https://doi.org/10.1016/j.jcat.2014.04.001.
[46] K. Mlekodaj, J. Dedecek, V. Pashkova, E. Tabor, P. Klein, M. Urbanova, R. Karcz, P. Sazama, S.R. Whittleton, H.M. Thomas, A.V. Fishchuk, S. Sklenak, Al Organization in the SSZ-13 Zeolite. Al Distribution and Extraframework Sites of Divalent Cations, J. Phys. Chem. C. 123 (2019) 7968–7987, https://doi.org/10.1021/acs.jpcc.8b07343.
[47] M. Lemishka, J. Dedecek, K. Mlekodaj, Z. Sobalik, S. Sklenak, E. Tabor, Speciation and siting of divalent transition metal ions in silicon-rich zeolites. An FTIR study, Pure Appl. Chem. 91 (2019) 1721–1732, https://doi.org/10.1515/pac-2018-1228.
[48] E. Tabor, G. Sádovská, M. Bernauer, P. Sazama, J. Nováková, V. Fíla, T. Kmječ, J. Kohout, K. Závěta, Z. Sobalík, Feasibility of application of iron zeolites for high-temperature decomposition of N2O under real conditions of the technology for nitric acid production, Appl. Catal. B 240 (2019) 358–366, https://doi.org/10.1016/j.apcatb.2017.11.014.
[49] G. Sadovska, E. Tabor, P. Sazama, M. Lhotka, M. Bernauer, Z. Sobalik, High temperature performance and stability of Fe-FER catalyst for N2O decomposition, Catal. Commun. 89 (2017) 133–137, https://doi.org/10.1016/j.catcom.2016.10.029.
[50] E. Tabor, K. Zaveta, N.K. Sathu, Z. Tvaruzkova, Z. Sobalik, Characterization of iron cationic sites in ferrierite using Mossbauer spectroscopy, Catal. Today 169 (2011) 16–23, https://doi.org/10.1016/j.cattod.2010.09.017.
[51] P. Sazama, B. Wichterlova, E. Tabor, P. Stastny, N.K. Sathu, Z. Sobalik, J. Dedecek, S. Sklenak, P. Klein, A. Vondrova, Tailoring of the structure of Fe-cationic species in Fe-ZSM-5 by distribution of Al atoms in the framework for N2O decomposition and NH3-SCR-NOx, J. Catal. 312 (2014) 123–138, https://doi.org/10.1016/j.jcat.2014.01.019.
[52] M. Wilke, F. Farges, P.-E. Petit, G.E. Brown, F. Martin, Oxidation state and coordination of Fe in minerals: an Fe K-XANES spectroscopic study, Am. Min. 86 (2001) 714–730, https://doi.org/10.2138/am-2001-5-612.
[53] T.E. Westre, P. Kennepohl, J.G. DeWitt, B. Hedman, K.O. Hodgson, E.I. Solomon, A multiplet analysis of Fe K-Edge 1s → 3d Pre-Edge features of iron complexes, J. Am. Chem. Soc. 119 (1997) 6297–6314, https://doi.org/10.1021/ja964352a.
[54] D. Wierzbicki, A.H. Clark, O. Kröcher, D. Ferri, M. Nachtegaal, Monomeric Fe species in square planar geometry active for low temperature NH3-SCR of NO, J. Phys. Chem. C. 126 (2022) 17510–17519, https://doi.org/10.1021/acs.jpcc.2c03480.
[55] U. Olsbye, S. Svelle, M. Bjorgen, P. Beato, T.V.W. Janssens, F. Joensen, S. Bordiga, K.P. Lillerud, Conversion of methanol to hydrocarbons: how zeolite cavity and pore size controls product selectivity, Angew. Chem. Int. Ed. 51 (2012) 5810–5831, https://doi.org/10.1002/anie.201103657.
[56] V.L. Sushkevich, R. Verel, J.A. van Bokhoven, Pathways of methane transformation over copper-exchanged mordenite as revealed by in situ NMR and IR spectroscopy, Angew. Chem. Int. Ed. 59 (2020) 910–918, https://doi.org/10.1002/anie.201912668.
[57] Z. Sobalík, J. Dědeček, D. Kaucký, B. Wichterlová, L. Drozdová, R. Prins, Structure, distribution, and properties of Co ions in ferrierite revealed by FTIR, UV–Vis, and EXAFS, J. Catal. 194 (2000) 330–342, https://doi.org/10.1006/jcat.2000.2926.
[58] B.R. Wood, J.A. Reimer, A.T. Bell, M.T. Janicke, K.C. Ott, Methanol formation on Fe/Al-MFI via the oxidation of methane by nitrous oxide, J. Catal. 225 (2004) 300–306, https://doi.org/10.1016/j.jcat.2004.04.010.